TIME-RESOLVED X-RAY DIFFRACTION STUDIES OF THE SARCOPLASMIC RETICULUM MEMBRANE DURING ACTIVE TRANSPORT

J. K. BLASIE,*‡ L. G. HERBETTE,*‡§ D. PASCOLINI,* V. SKITA,* D. H. PIERCE,* AND A. SCARPA*

*Departments of Chemistry and Biochemistry/Biophysics, University of Pennsylvania, Philadelphia, Pennsylvania; ‡Department of Biology, Brookhaven National Laboratory, Upton, New York; and §Department of Medicine, University of Connecticut Health Center, Farmington, Connecticut

ABSTRACT X-ray and neutron diffraction studies of oriented multilayers of a highly purified fraction of isolated sarcoplasmic reticulum (SR) have previously provided the separate profile structures of the lipid bilayer and the Ca^{2+}-ATPase molecule within the membrane profile to ~10-Å resolution. These studies used biosynthetically deuterated SR phospholipids incorporated isomorphously into the isolated SR membranes via phospholipid transfer proteins. Time-resolved x-ray diffraction studies of these oriented SR membrane multilayers have detected significant changes in the membrane profile structure associated with phosphorylation of the Ca^{2+}-ATPase within a single turnover of the Ca^{2+}-transport cycle. These studies used the flash photolysis of caged ATP to effectively synchronize the ensemble of Ca^{2+}-ATPase molecules in the multilayer, synchrotron x-radiation to provide 100–500-ms data collection times, and double-beam spectrophotometry to monitor the Ca^{2+}-transport process directly in the oriented SR membrane multilayer.

INTRODUCTION

The ATP-driven active transport of calcium across the sarcoplasmic reticulum (SR) membrane in muscle decreases the cytosolic Ca^{2+} concentration, thereby inducing the physiological relaxation of the myofibrils (1–3). Extremely pure fractions of rabbit skeletal SR can be isolated in the form of sealed, unilamellar vesicles; these homogenous vesicular dispersions contain essentially only phospholipid and the Ca^{2+}-ATPase protein (>90% of the total protein with ~10^5 MW) and are highly functional in terms of their ATP-induced Ca^{2+} uptake and possibly also their Ca^{2+}-release properties (4–8). We have shown that these vesicular dispersions of isolated light SR can be formed into hydrated multilayers composed of highly oriented stacks of the flattened unilamellar vesicles (5, 9).

These oriented multilayers of isolated light SR give rise to extensive lamellar x-ray and neutron diffraction; the separate profile structures (i.e., the structures projected onto the normal to the membrane plane) of the phospholipid bilayer and the Ca^{2+}-ATPase molecule within the SR membrane profile have recently been derived to ~10-Å resolution (see references 10–14 for details) and are shown in Fig. 1. The derivation of these separate profile structures required the utilization of biosynthetically deuterated SR phospholipids incorporated isomorphously (isomorphism was verified by x-ray diffraction [~10-Å resolution], freeze-fracture electron microscopy and ATP-induced Ca^{2+}-transport) into the isolated SR membranes via phospholipid transfer proteins. The lamellar neutron diffraction data from the oriented multilayers of SR membranes containing the deuterated SR lipids (phosphatidylcholine [PC] only or phosphatidylcholine and phosphatidylethanolamine [PE]) were analyzed to provide directly, by appropriate difference methods, the PC and PC + PE bilayer profiles within the SR membrane profile to ~30 Å resolution. The electron density profile of the SR membrane derived directly from lamellar x-ray diffraction data from oriented multilayers was subjected to a highly constrained model refinement analysis to provide the separate electron density profile for the phospholipid bilayer and profile structure for the Ca^2-ATPase molecule expressed as an area profile within the SR membrane profile to ~10-Å resolution; the more crucial constraints were provided by the lower resolution phospholipid bilayer and water distribution profiles within the SR membrane profile provided by the neutron diffraction analysis and the membrane lipid-to-protein ratio. The lipid bilayer within the SR membrane is seen to be substantially asymmetric with regard to (*a*) the average fatty-acyl chain extension of phospholipid molecules in the two monolayers of the bilayer (differing by ~20%) with an average polar headgroup separation of ~40 Å across the bilayer profile and (*b*) the relative number of phospholipid molecules in the inner monolayer (facing the intravesicular water space), namely, 54 ± 1% vs. the outer monolayer (facing the

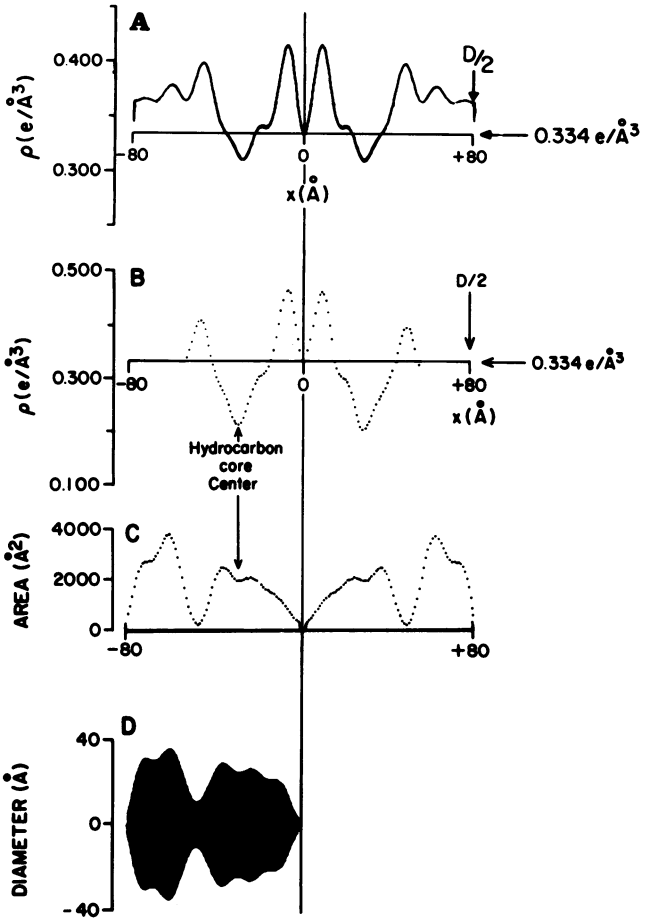

FIGURE 1 A summary of the results of structural studies of the SR membrane profile at ~10-Å resolution using a combination of x-ray and neutron diffraction techniques as taken from reference 14. *A* contains the electron density profile on an absolute scale for the unit cell of the oriented SR membrane multilayer containing the two apposed single-membrane profiles of the flattened unilamellar SR vesicle; a single-membrane profile is contained within the interval 0 Å $\leq |x| \leq$ 80 Å. *B* contains the separate electron density profile on an absolute scale for the asymmetric lipid bilayer within the SR membrane profile for 0 Å $\leq |x| \leq$ 80 Å. *C* contains the separate protein profile within the SR membrane profile for 0 Å $\leq |x| \leq$ 80 Å expressed as the area occupied by the protein in the membrane plane as,a function of the profile coordinate x. This protein area profile can also be expressed as a protein diameter profile (*D*) for the SR membrane protein structure cylindrically averaged about the normal to the membrane plane.

extravesicular water space), namely, 46 ± 1%, i.e., a distributional asymmetry of 8 ± 1%. The Ca^{2+}-ATPase molecular profile within the SR membrane is seen to span the lipid bilayer extending from $|x| \sim 5$ Å to $|x| \sim 60$ Å in the SR membrane profile with a substantial portion of its mass occurring outside of the lipid polar headgroups on the extravesicular side of the SR membrane profile, i.e., from $|x| \sim 60$ Å to $|x| \sim 80$ Å. About 27% of the total Ca^{2+}-ATPase mass occurs within the inner monolayer of the lipid bilayer, ~24% occurs within the outer monolayer and the remaining 49% occurs outside the lipid bilayer on the extravesicular surface of the SR membrane profile. While ~50% of the Ca^{2+}-ATPase mass occurs within the lipid bilayer (including the phospholipid headgroup regions) in the SR membrane profile, only ~40% of the total Ca^{2+}-ATPase mass occurs within the hydrocarbon core of the lipid bilayer, with the protein occupying a significantly greater average area within the plane of the outer monolayer as compared with the inner monolayer.

A crucial aspect of this research concerns the Ca^{2+} transport properties of the isolated SR membranes within these oriented multilayers used in the structural studies. We have directly demonstrated that SR membranes (whose protein content is ~65% Ca^{2+}-ATPase) within such hydrated oriented multilayers are fully capable of ATP-induced Ca^{2+}-transport, and that the Ca^{2+}-transport properties of the less pure SR membranes are essentially identical to those of a highly purified fraction of SR membranes (whose protein content is >90% Ca^{2+}-ATPase) when the transport properties are normalized to the amount of SR protein actually phosphorylated (i.e., the Ca^{2+}-ATPase). These studies of Ca^{2+}-transport kinetics used double-beam spectrophotometric techniques and arsenazo III to detect the Ca^{2+}-transport process and the laser flash photolysis of caged ATP (15) to effectively synchronize the Ca^{2+}-transport cycles among the ensemble of Ca^{2+}-ATPase molecules in the oriented multilayer (16–18). The kinetics of ATP-induced Ca^{2+}-transport in the oriented multilayers over the temperature range $-1°C \leq T \leq 21°C$ are essentially identical to those of the vesicular dispersions. In Fig. 2 (adapted from reference 17) the Ca^{2+}-transport kinetics for the multilayers and dispersions are compared over the respective temperature ranges $-1°C \leq T \leq 21°C$ and $-2° \leq T \leq 26°C$. In both cases, the transport kinetics exhibit a Ca^{2+}-ionophore insensitive fast phase (first order with initial rates of 10^2–10^3 nmol Ca^{2+}/mg ATPase/s over the temperature range with an activation energy of $E_a \sim 16$ kcal/mol) and a Ca^{2+}-ionophore sensitive slow phase (first order with initial rates of 10^0 10^2 nmol Ca^{2+}/mg ATPase/s over the temperature range with an activation energy of $E_a \sim 22$ kcal/mol). The fast phase has a stoichiometry of ~2 mol Ca^{2+}/1 mol phosphorylated enzyme, whereas the slow phase has a stoichiometry of ~2 mol Ca^{2+}/1 mol ATP hydrolyzed. The Ca^{2+}-ionophore insensitive fast phase has kinetics essentially identical to those for the formation of the ADP-sensitive, acid-stable phosphorylated enzyme intermediate (as determined independently by a quenched-flow technique) and may therefore be consistent with either an ATP-induced increase in the affinity of two Ca^{2+} binding sites on the enzyme or an ATP-induced occlusion of two Ca^{2+} binding sites on the enzyme, resulting in their inaccessibility from either surface of the SR membrane. The slow phase may be identified with the translocation of Ca^{2+} across the membrane profile due to its Ca^{2+}-ionophore sensitivity and its relatively high activation energy. However, other kinetic

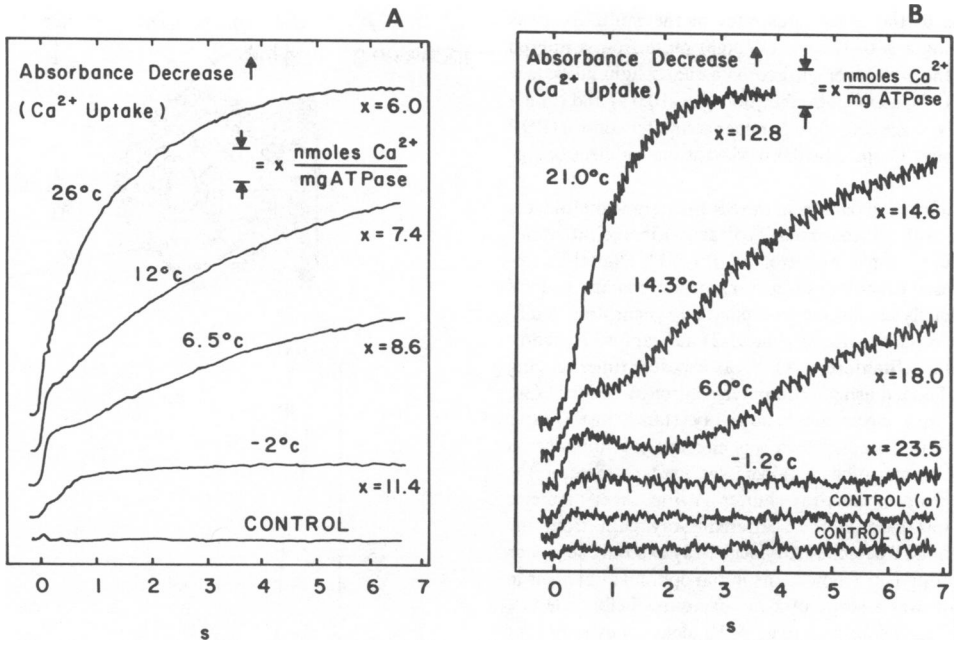

FIGURE 2 A summary of the results taken from reference 17 of calcium uptake kinetics experiments on unilamellar SR vesicles in dispersions (*A*) and in partially dehydrated oriented multilayers (*B*) as a function of temperature. The extravesicular calcium concentration was monitored spectrophotometrically using a metallochromic dye and calcium transport was initiated via the laser flash photolysis of caged ATP. Caged ADP (*a*) or no-nucleotide (*b*) served as controls. At least two kinetic phases of calcium uptake occur in both SR membrane systems (see text and reference 17).

phases of the Ca^{2+}-transport process may be indicated by the somewhat greater lag between the fast and slow phase that is more readily apparent in the oriented multilayers.

The nature of the time-resolved x-ray diffraction studies of the SR membrane can be summarized briefly as follows: The overall Ca^{2+}-transport process is initiated essentially synchronously through the ensemble of Ca^{2+}-ATPase molecules within an oriented multilayer of isolated SR membranes via the flash photolysis of caged ATP. The time scale of the effective synchronization of the ensemble depends initially upon the duration of the ultraviolet (UV) light flash required to produce a sufficient quantity of ATP in the multilayer to sustain several turnover cycles of the Ca^{2+}-ATPase molecules and is ultimately limited to the millisecond time scale due to the kinetics of the dark reactions of the photolysis process (15). Lamellar (meridional) x-ray diffraction is recorded from the multilayer prior to the flash photolysis and after a variable delay τ following the flash photolysis using x-ray exposure times that are short compared with the turnover time (16, 17) of the Ca^{2+}-transport cycle, which is on the order of a few seconds at 6–8°C. Such diffraction patterns can then be used to investigate changes within the profile structure of the SR membrane occurring at different times (different τ's) within the calcium transport cycle and these changes can ultimately be correlated with the various chemical intermediates in the cycle (16–18). The flash photolysis of caged ADP under otherwise identical experimental circumstances provides an essential control to these studies since the same amount of light energy is absorbed by the multilayer and similarly dissipated without producing a high-energy substrate for the Ca^{2+}-ATPase. The ultimate time resolution required of such studies depends upon the lifetimes of the various intermediates in the transport cycle under the experimental conditions employed. The ultimate time resolution achievable depends both upon the rate of ATP production by the flash-photolysis mechanism (currently limited to the millisecond time scale by the kinetics of the dark reactions using a pulsed laser UV source) and the incident x-ray flux (currently limited to the nanosecond or millisecond time scales using laser plasma or synchrotron x-ray sources, respectively).

METHODS

Oriented multilayers of isolated, highly purified SR (Ca^{2+}-ATPase content >90% of the total protein with $\sim 10^5$ mol wt) were prepared on aluminum foil and mounted on cylindrically curved glass supports as previously described (5, 9) with the exception that the final sedimentation medium also contained sufficient caged ATP or caged ADP to produce a final caged-substrate/Ca^{2+}-ATPase mole ratio of 1–2 in the multilayer after partial dehydration. The resulting cylindrically curved multilayers were mounted in identical canisters with aluminum foil x-ray entrance and exit windows for grazing x-ray incidence to the multilayer surface and a Saran window for the UV-photolysis light incident normal to the multilayer surface; these canisters were each reproducibly positioned in a temperature-regulated (7–8°C ± 0.1°C) water-cooled chamber possessing appropriate ports to match the three canister windows. Humidity was controlled via a saturated salt solution in the sealed canisters.

The flash photolysis of the caged substrates in the multilayer was effectively achieved using a 300–370 nm UV light pulse from a filtered Hg-arc transmitted to the multilayer surface via a quartz light guide (see reference 17 for details). The UV pulse duration (0.1–10.0 s) and timing relative to the x-ray pulses (see below) were under computer control (PDP 11/34; Digital Equipment Corp., Marlboro MA) using an electromagnetic UV shutter.

The lamellar x-ray diffraction data from the SR membrane multilayers were recorded with an SIT (silicon intensified target) image intensifier x-ray detector (21) under computer control (PDP 11/34; Digital Equipment Corp.) using focused (double-bent mirror) monochromatic (~1 eV bandwidth via a Ge doubly-crystal monochromator) synchrotron radiation (8048 eV) from a bending magnet (line II-2) at Stanford Synchrotron Radiation Laboratory (Stanford, CA). X-ray exposure times ranging from 0.1–10.0 s were obtained using a computer-controlled (PDP 11/34; Digital Equipment Corp.) electromagnetic x-ray (tantalum) shutter placed in the incident x-ray beam, which was effectively continuous on this time scale. A short ionization chamber was used to monitor the average x-ray flux incident on the x-ray shutter. A 4 in. inner-diameter evacuated beampipe was used in the scattered x-ray path from the specimen chamber to the SIT detector. A typical x-ray exposure sequence on an SR membrane multilayer following its initial optimal alignment in the incident x-ray beam was a series of x-ray exposures before the UV flash photolysis of the caged substrate (e.g., 5–10 identical exposures of 0.2–1.0 s each to subsequently check the lamellar diffraction from the multilayer for instabilities arising from the multilayer, detector, and/or incident x-ray beam) and a repetition of that series of x-ray exposures following the UV flash photolysis by a delay $\tau \geq 0$ s (e.g., 5–10 identical exposures also of 0.2–1.0 s each to probe transient substrate-induced changes in the lamellar diffraction from the multilayer). The same series of x-ray exposures was repeated again several minutes after the UV flash photolysis for comparison with the first series of exposures before the UV flash. An automatic delay of ~14 s occurred between each x-ray exposure in the sequences before and after the UV flash due to the SIT detector read-out cycle.

These lamellar diffraction data obtained as two-dimensional digital data arrays for each exposure were integrated over the mosaic spread of the data to provide the one-dimensional lamellar intensity function $I(s)$ where $s = (2 \sin \theta)/\lambda$ as described previously (9, 22). These lamellar intensity functions could be compared directly with others in the same or following sequences via direct arithmetic differences using identical integration parameters. Selected (see Results) lamellar intensity functions were subjected to a Fourier analysis, which takes into proper account the various possible forms of disorder present in the multilayer lattice (5, 9, 23). The low-resolution electron density profiles for a single SR membrane resulting from these Fourier analyses were then subjected to a step-function model refinement procedure (14, 22, 24) to more accurately assess the differences between appropriate (see Results) single membrane profiles.

RESULTS

The lamellar x-ray diffraction typical for these oriented multilayers of isolated light SR membranes is shown in Fig. 3 *a* as a contour plot of counts vs. position on the SIT detector active area; the integration limits are also shown for the integration over the small mosaic spread of the lamellar diffraction to produce the lamellar intensity function $I(s)$ shown in Fig. 3 *b*. The lamellar intensity function contains the first seven orders of lamellar diffraction exhibiting the significant effects of lattice disorder (of the second kind [23]) for a multilayer lattice periodicity of ~200 Å.

The results of a typical time-resolved x-ray diffraction

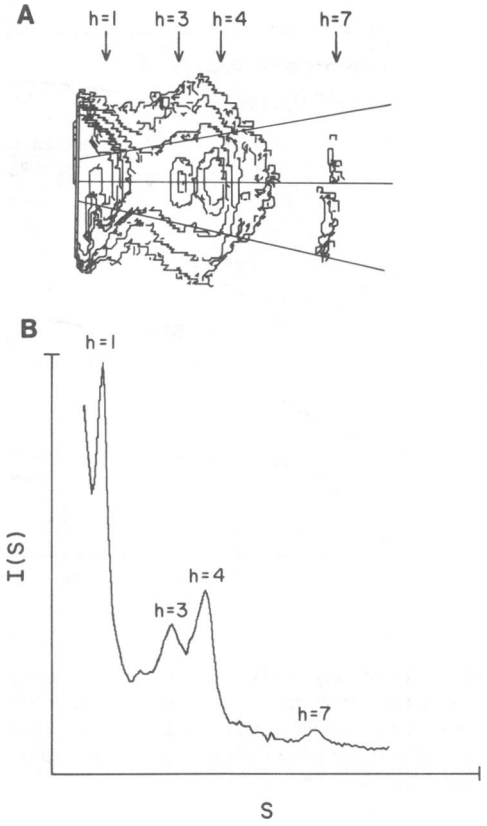

FIGURE 3 A typical lamellar x-ray diffraction pattern from a partially dehydrated, oriented SR membrane multilayer obtained with synchrotron x-radiation and an SIT image-intensifier x-ray detector (see text). The low-angle portion of the lamellar diffraction is shown as a contour plot of counts vs. position on the detector active area (only a few selected contour levels are shown for clarity) in *A*; peaks corresponding to the diffraction orders $h = 1, 3, 4, 7$ are indicated. Integration of this two-dimensional lamellar diffraction over the small mosaic spread between the limits indicated in *A* results in the lamellar intensity function $I(s)$ shown in *B*, which contains intensity maxima for the lamellar diffraction orders $h = 1, 2, 3, 4$, and 7 as indicated.

experiment are shown in Fig. 4. Fig. 4 *a* displays the lamellar intensity function $I(s)$ from a partially dehydrated oriented multilayer of isolated light SR membranes recorded with a 0.5-s x-ray exposure immediately before the UV flash photolysis of caged ATP in the multilayer; all such similar exposures before this in the series before the UV flash photolysis provided lamellar intensity functions that were identical to that shown within the experimental noise, indicative of multilayer, SIT detector, and incident x-ray beam stability. Fig. 4 *b* displays the lamellar intensity function from the same multilayer immediately after a 0.25-s UV flash ($\tau = 0$ s) recorded with a 0.5-s x-ray exposure; the next few (2–3) x-ray exposures (0.5 s each) in the series after the UV flash provided lamellar intensity functions similar to that shown in Fig. 4 *b*. 1 min or more after the UV flash, 0.5-s x-ray exposures in the series provided the lamellar intensity function displayed in Fig. 4 *c*. The numerically smoothed versions of Fig. 4 *a–c* are

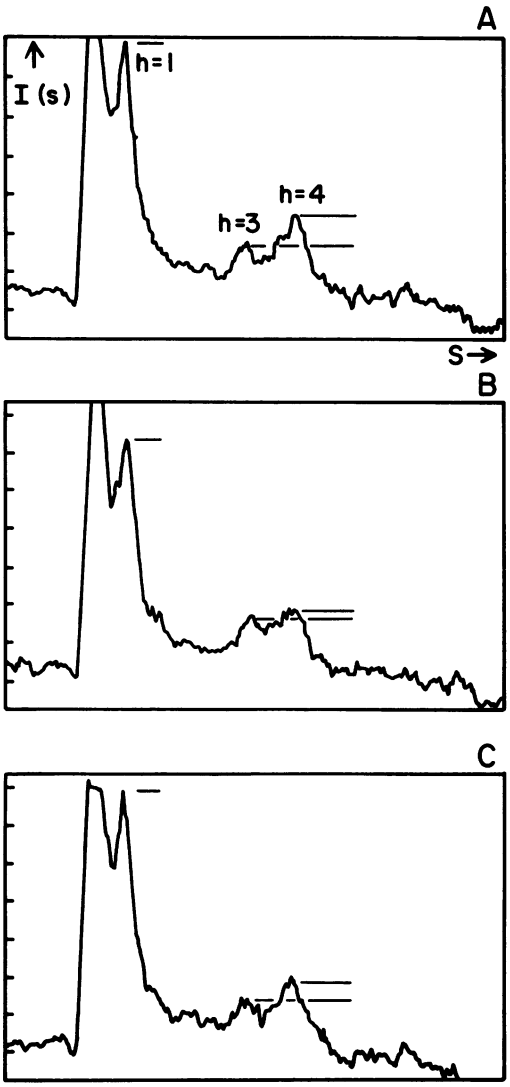

FIGURE 4 Typical lamellar intensity functions obtained from partially dehydrated, oriented SR membrane multilayers ($D \sim 200$ Å) containing caged ATP, each recorded with 0.5-s exposures using focused, monochromatic synchrotron x-radiation and an SIT image-intensifier x-ray detector, immediately before a 0.25 s UV flash (*A*), immediately after the UV flash, i.e., $\tau = 0$ s (*B*), and 1 min after the UV flash (*C*). Significant differences in the relative intensities of the lamellar diffraction orders $h = 1, 3, 4$ are readily apparent in *B* as compared with *A* and *C*. The close similarity of the lamellar intensity functions of *A* and *C* indicate the full reversibility of the ATP-induced changes evident in the lamellar intensity function of *B* following the exhaustion of the ATP produced via the flash photolysis of caged ATP. No such significant changes were ever observed using the flash photolysis of caged ADP in place of caged ATP under otherwise identical experimental conditions.

displayed in Fig. 5 *a–c*. Arithmetic differences between selected pairs of these lamellar intensity functions shown in Figs. 4 and 5 are given in Fig. 6.

The results shown in Figs. 4, 5, and 6 clearly indicate that reversible changes in the first seven orders of lamellar diffraction from this SR membrane multilayer were induced by the flash photolysis of caged ATP (caged ATP/ATPase mole ratio ≃2) in the multilayer; these reversible changes are all substantially greater than the magnitude of the local experimental errors of x-ray detection over the SIT detector active area. Qualitatively similar results have been reproducibly[1] obtained with 0.2-s and 0.4-s x-ray exposures for each series and UV-flash durations of 0.1 s and 0.2 s, respectively, for $\tau = 0$ s. No changes in the lamellar diffraction from such multilayers have ever been observed using caged ADP in place of caged ATP (all other conditions being completely equivalent) within the experimental errors of x-ray detection over this range of $s = (2 \sin \theta)/\lambda$ (e.g., see Fig. 6).

The lamellar intensity functions of Figs. 4 *a* and *b* were subjected to the direct analysis (so-called GFSDM) described in reference 23 using the same estimated lamellar background scattering function (9) for each. This analysis indicated that the flash photolysis of caged ATP in the multilayer initially ($\tau = 0$ s) induced (*a*) a negligible change in the multilayer lattice periodicity of less than ±0.5 Å, (*b*) possibly a slight increase (1–2 Å) in the average separation of the two apposed single membrane profiles of the flattened vesicle across the intravesicular water space in the unit cell profile, and (*c*) small, but experimentally significant changes throughout most of the low-resolution (~29 Å) single-membrane electron density profile shown in Fig. 7 (i.e., a loss of electron density in the vicinity of $x \sim \pm 60$ Å corresponding to the extravesicular surface of the membrane and an increase of density both in the vicinity of $x \sim 0$ Å corresponding to the intravesicular surface of the membrane and in the vicinity of $x \sim \pm 30$ Å corresponding to the hydrocarbon core region of the membrane lipid bilayer). Because of the inherent low resolution of the two resulting single-membrane profiles of Fig. 7, they were subjected to a step-function model refinement analysis, which was necessarily modified with respect to that described in references 14, 22, and 24 to more accurately describe the small but experimentally significant differences between these two membrane profiles. These modifications took into account that the higher-resolution (~10 Å) single-membrane profile before ATP-induced calcium transport had already been uniquely modeled in terms of the separate profiles of its protein, lipid, and water components as described in the Introduction; therefore, their lower resolution (~29 Å) counterparts were also already known. The changes in the average

[1]The reproducibility of these time-resolved x-ray diffraction results from multilayer to multilayer is comparable to those results obtained in kinetic studies of ATP-induced Ca^{2+} uptake (17); namely, at least 50% of the multilayers exhibit ATP-induced effects. When ATP-induced effects are obtained in either case, they are all qualitatively similar. The Ca^{2+}-transport system in these isolated, highly purified SR membrane multilayers is somewhat labile over the temperature and hydration ranges employed (17), and this lability is presumably responsible for the multilayer reproducibility observed by us in these two kinds of experiments.

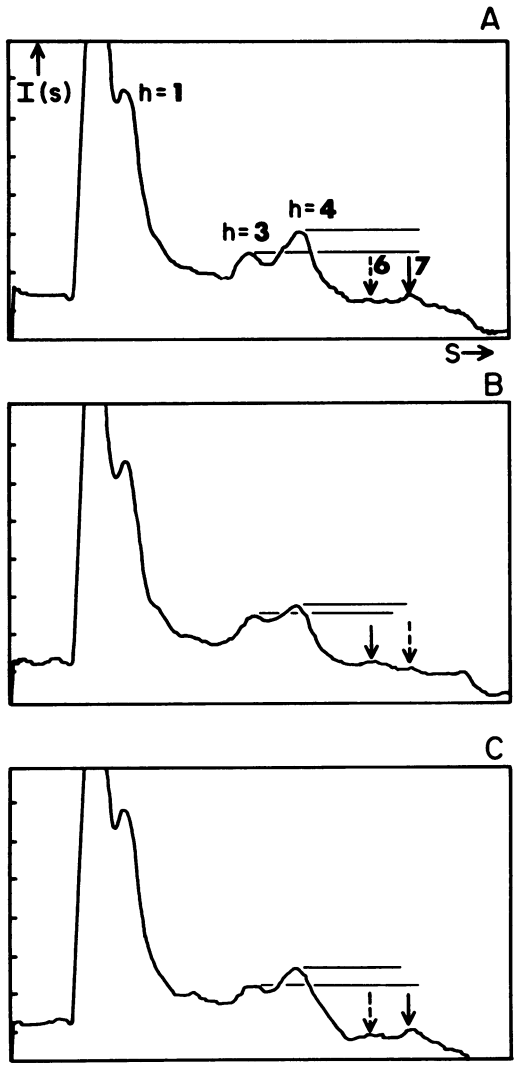

FIGURE 5 Same as Fig. 4, except that a consecutive-channel, numerical smoothing procedure has been uniformly applied to the lamellar intensity functions of Fig. 4. Additional differences in the relative intensities of the lamellar diffraction orders $h = 6, 7$ are also readily apparent in *B* as compared with *A* and *C*. The close similarity of the lamellar intensity functions of *A* and *C* indicate the full reversibility of the ATP-induced changes evident in the lamellar intensity function of *B* following the exhaustion of the ATP produced via the flash photolysis of caged ATP. No such significant changes were ever observed when caged ADP replaced caged ATP in the multilayers under otherwise identical conditions.

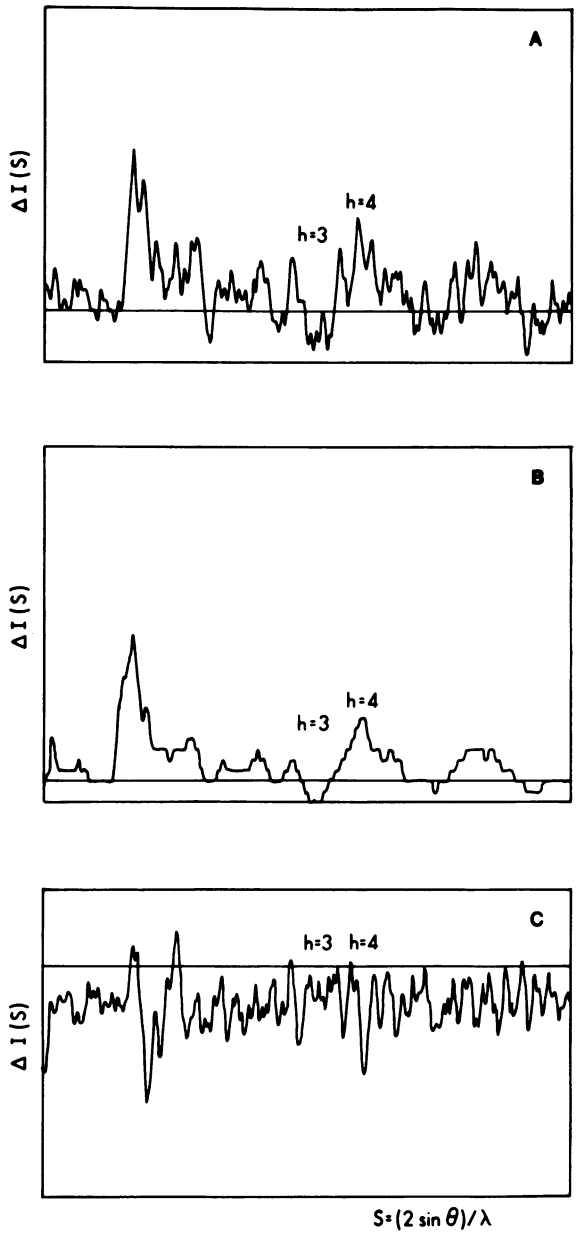

FIGURE 6 If the arithmetic difference of the intensity functions of Figs. 4 *A* and 4 *B*, 5 *A* and 5 *B* are calculated, one obtains respectively Fig. 6 *A* (i.e., 4 *A*–4 *B*) and 6 *B* (i.e., 5 *A*–5 *B*). Fig. 6 *C* is otherwise equivalent to Fig. 6 *A*, except that the multilayer contained caged ADP instead of caged ATP.

electron density levels of the various features of the lower-resolution single-membrane profile labeled (1–4 in Fig. 8) induced by ATP were then modeled considering only possible changes in the protein profile structure, possible changes in the average conformation of the phospholipid molecules in each monolayer of the lipid bilayer and the resulting possible changes in the water profile structure; the possibility of phospholipid "flip-flop" was not considered in view of the time scale (<0.5 s) of the observed structural changes in the membrane profile. The results of this model refinement analysis are shown in Fig. 8. The step-function profiles of Fig. 8 *a* fit (normalized least-squares difference integrated over $0 \text{ Å} \leq x \leq D/2$) their respective continuous profiles of Fig. 7 to better than 0.2%. The difference step-function profile (Fig. 8 *b*) for the various features of the single-membrane profile clearly indicates the detailed nature of the loss of mass from the extravesicular surface of the membrane profile (regions 3 and 4) and its conservative redistribution into the lipid hydrocarbon core (region 2) and intravesicular surface (region 1) of the membrane profile arising primarily from ATP-induced changes in the protein profile structure.

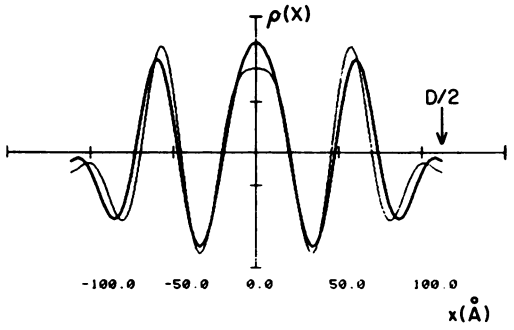

FIGURE 7 Unit cell electron density profiles at relatively low resolution (~29 Å) calculated directly (see text) from the phased lamellar intensity functions of Fig. 4; a single-membrane profile is contained within 0 Å $\leq |x| \leq$ 100 Å. The lighter line corresponds to the SR membrane profile (averaged over a 0.5-s interval) immediately before the UV flash photolysis of caged ATP in the oriented multilayer while the heavier line corresponds to the membrane profile (averaged over a 0.5-s interval) immediately after the UV flash photolysis, τ = 0 s. The differences between these two membrane profiles (see text) are experimentally significant in terms of the errors in the experimental intensity functions of Fig. 4 from which they were derived.

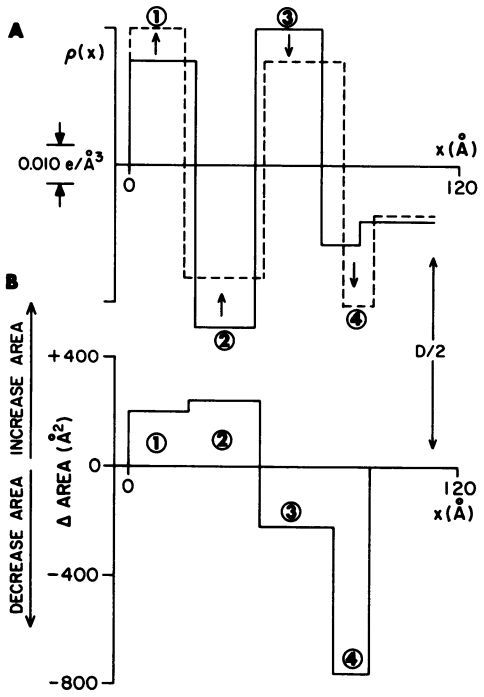

FIGURE 8 (*A*) Refined step-function model profiles on an absolute electron density scale for the continuous unscaled single-membrane profiles shown in Fig. 7 (see text for details). The solid line corresponds to the SR single-membrane profile immediately before the UV flash photolysis of caged ATP in the multilayer while the dashed line corresponds to that immediately following the UV flash photolysis, τ = 0 s. (*B*) The differences of the electron density levels within regions 1–4 of the two membrane profiles shown in *A* are expressed as a difference in the SR membrane protein area profiles for these four regions of the membrane profile (see text). These differences in the protein area profile conserve SR protein mass and correspond to changes in the SR protein structure upon phosphorylation before calcium transport across the membrane profile (200–500-ms time resolution; see text).

DISCUSSION

Time-resolved Studies within a Single Turnover

The results of the time-resolved x-ray diffraction experiments described above indicate that ~8% (~13,000 Å^3) of the total mass of the Ca^{2+}-ATPase (~157,000 Å^3) is redistributed from the extravesicular surface to the lipid hydrocarbon core and intravesicular surface regions of the SR membrane profile within the first 0.2–0.5 s at 7–8°C following the flash photolysis of caged ATP in the multilayer. This relatively large-scale redistribution of protein mass must be induced by ATP itself since the photolysis dark reactions occur on the millisecond time scale (15) under the conditions of these experiments and since the flash photolysis of caged ADP under otherwise identical experimental conditions induces no such structural changes in the SR membrane profile at this resolution. We have assumed that these ATP-induced structural changes cannot arise from phospholipid "flip-flop" because of the locations of the changes in the membrane profile coupled with the time scale on which they occur (i.e., too fast for phospholipid "flip-flop").

Comparing the results of these time-resolved x-ray diffraction studies with those results of the kinetic studies of ATP-induced Ca^{2+} uptake in such oriented multilayers of isolated SR membranes at 7–8°C (see references 16, 17, and Fig. 2 *B* for the temperature 6°C), it is readily apparent that the structural changes described occur within the first turnover of the essentially synchronous ensemble of Ca^{2+}-ATPase molecules in the multilayer and are associated with the ATP-induced phosphorylation of the Ca^{2+}-ATPase coupled with the occlusion of two Ca^{2+} ions/ATPase molecule.

Time-resolved Studies Averaged over Several Turnovers

Otherwise identical time-resolved x-ray diffraction studies on such oriented multilayers of isolated SR membranes have also been performed by us using longer x-ray exposure times of 1.5–5.0 s afforded by both synchrotron and rotating-anode (GX-6; Elliott Brothers, London, England) x-ray sources. The results of a typical experiment using 5.0 s x-ray exposure times, a rotating-anode x-ray source and a linear position-sensitive x-ray detector are shown in Fig. 9 for a multilayer at a somewhat smaller lattice periodicity of ~160 Å, T = 7–8°C ± 0.1°C and τ = 0 s. Similar analyses of these data are shown in Fig. 10 at a resolution somewhat greater than that of the synchrotron radiation experiments. It is interesting to note that the ATP-induced changes in the SR single-membrane profile are similar to those described above using synchrotron radiation and 0.2–0.5 s exposure times. During this time window of 5 s (τ = 0 s), the ensemble of Ca^{2+}-ATPase molecules in the multilayer has progressed through several turnovers of the

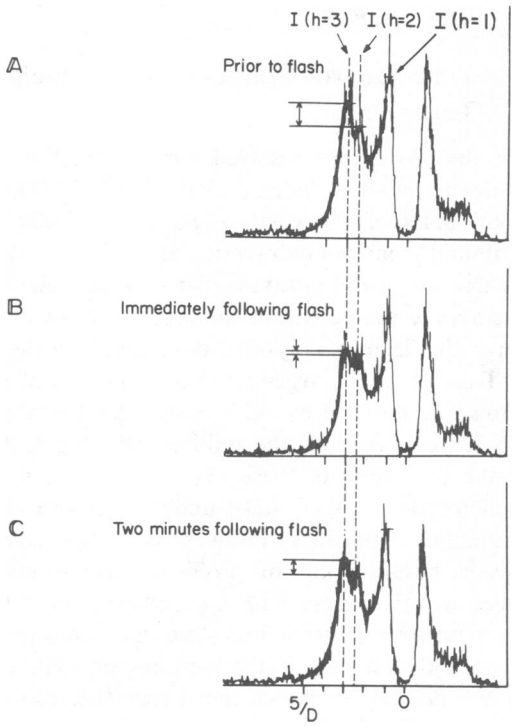

FIGURE 9 Typical lamellar intensity functions obtained from partially dehydrated, oriented SR membrane multilayers ($D \sim 160$ Å) containing caged ATP, each recorded with 5.0-s exposures using focused, Ni-filtered CuKα x rays from a rotating-anode source and a linear position-sensitive x-ray detector, immediately before a 1-s UV flash (*A*), immediately after the UV flash, i.e., $\tau = 0$ s, (*B*), and 2 min after the UV flash (*C*). Significant differences in the relative intensities of the lamellar diffraction orders $h = 1, 2, 3$ are readily apparent in *B* as compared with *A* and *C*. The close similarity of the lamellar intensity functions of *A* and *C* indicate the full reversibility of the ATP-induced changes evident in the lamellar intensity function of *B* following the exhaustion of the ATP produced via the flash photolysis of caged ATP. No such significant changes were ever observed using the flash photolysis of caged ADP in place of caged ATP under otherwise identical experimental conditions.

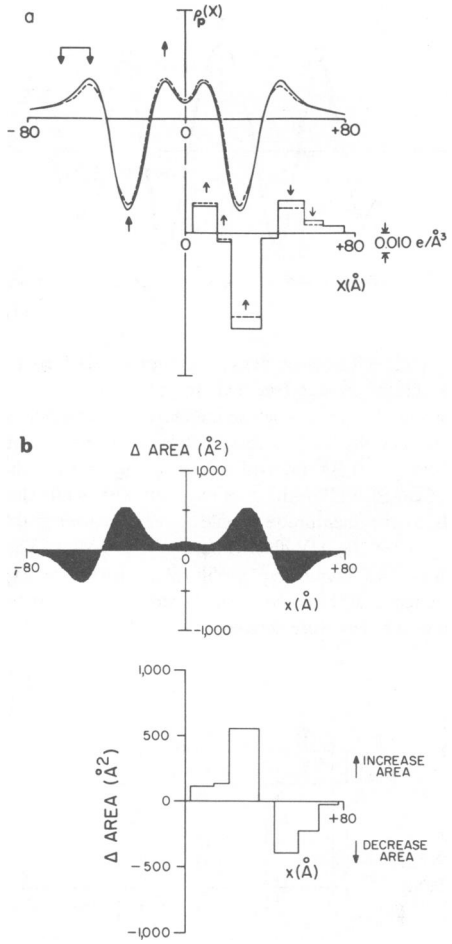

FIGURE 10 (*a*) Unit cell electron density profiles at relatively low resolution (~25 Å) calculated directly (see text) from the phased lamellar intensity functions of Fig. 9; a single membrane profile is contained within $0 \text{ Å} \leq |x| \leq 80$ Å. The solid line corresponds to the SR membrane profile (averaged over a 5.0-s interval) immediately before the UV flash photolysis of caged ATP in the oriented multilayer while the dashed line corresponds to the membrane profile (averaged over a 5.0-s interval) immediately after the UV flash photolysis, $\tau = 0$ s. The refined step-function models corresponding to these continuous single-membrane profiles are also shown, respectively. The differences between these two membrane profiles (see text) are experimentally significant in terms of the errors in the experimental intensity functions of Fig. 9 from which they were derived. (*b*) The differences in the single-membrane electron-density profiles shown in *a* are expressed as a difference in the SR membrane protein area profile (see text). These differences in the protein area profile conserve SR protein mass and correspond to changes in the SR protein structure averaged over more than one turnover of the calcium transport cycle (5-s time resolution; see text).

Ca^{2+}-transport cycle at 7–8°C (see references 16, 17, and Fig. 2 *b*). Hence, the ATP-induced changes in the SR membrane profile averaged over several turnovers of the ensemble's transport cycles are similar to those changes in the SR membrane profile associated with the phosphorylation of the Ca^{2+}-ATPase described above (Fig. 11). This phenomenon would occur if indeed this acid-stable, ADP-sensitive phosphorylated enzyme intermediate (or other enzyme intermediates leading to its formation following the flash photolysis of caged ATP) were the longest lived or predominant intermediate(s) in the Ca^{2+}-transport cycle under the conditions of these experiments, namely, oriented SR membrane multilayers at 7–8°C. In the scheme of deMeis (20), this would imply that the $E \sim P$ to $E^* \sim P$ transition, critical to calcium translocation across the membrane profile, is the rate-limiting step in the Ca^{2+}-transport cycle under the conditions of these experiments. This conclusion is also supported by a recent independent study of the time-dependent distribution of intermediate states in the Ca^{2+}-transport cycle (27); pertinent to this work, Fernandez-Belda et al. report an excess of the E' to the E^* form of the enzyme (see reference 27 for their specific notation) of 2:1 at 25°C in vesicular dispersions noting that the ratio of E' to E^* would be expected to be substantially greater than this value of 2:1 at 7–8°C in oriented SR membrane multilayers (16, 17).

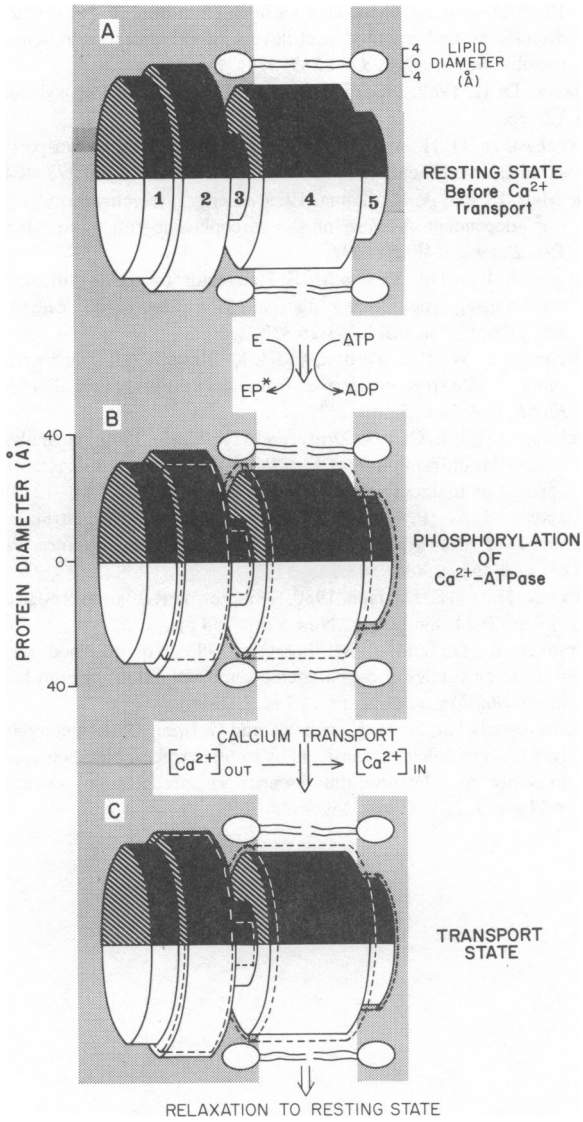

FIGURE 11 Schematic representations of the cylindrically averaged (about the normal to the membrane plane) SR membrane protein structure at relatively low resolution (~29 Å) before calcium transport (*A*), in the phosphorylated intermediate state of the calcium ATPase (see text for details) as derived from the synchrotron radiation studies with 0.2–0.5-s time resolution (*B*), and in the averaged calcium transport state as derived from the rotating-anode x-ray studies with 5.0-s time resolution (*C*). Five cylindrical regions were used to represent the Ca^{2+}-ATPase at this resolution as labeled in *A*. In both *B* and *C*, the dashed-line cylinders represent the "new" state of the Ca^{2+}-ATPase as indicated superimposed on the "resting" state (solid line cylinders) of *A*. For both *B* and *C*, regions 2 and 3 decrease in volume, which is conservatively gained in regions 4 and 5. Thus, the phosphorylated state (see text for details) and the average Ca^{2+}-transport state of the Ca^{2+}-ATPase were similar to each other and different from the resting state (see text).

CONCLUSION

We have developed the techniques nececessary to investigate larger-scale structural changes within the SR membrane occurring within a single turnover of the effectively synchronous Ca^{2+}-transport cycles of the ensemble of Ca^{2+}-ATPase molecules in the oriented membrane multilayer. We have now reported such structural changes in the membrane profile associated with the phosphorylation of the Ca^{2+}-ATPase and the coupled occlusion of two Ca^{2+} ions per ATPase molecule following the flash photolysis of caged ATP in the multilayer. The time resolution of these x-ray diffraction studies can be considerably improved to the 1-ms time scale using a pulsed laser for the flash photolysis of caged ATP (16, 17) and either a wiggler-magnet synchrotron radiation (25) or a laser plasma (26) x-ray source. This improved time resolution would enable us to probe the kinetics of the larger scale structural changes in the SR membrane associated with the formation and decay of the high-energy phosphorylated intermediate and other states of the calcium ATPase occurring within the Ca^{2+}-transport cycle. This improved time resolution is currently limited only by the kinetics of the flash photolysis dark reactions of this particular caged ATP substrate (14).

This work was supported by a National Institutes of Health (NIH) grant HL-18708 to J. K. Blasie and A. Scarpa, and by grants from NIH (HL-27630, HL-32588) and the American Heart Association (with partial support by the Connecticut affiliate) to L. Herbette. L. Herbette is a Charles E. Culpepper Foundation Fellow.

Received for publication 18 October 1984 and in final form 13 February 1985.

REFERENCES

1. Ebashi, S., M. Endo, and I. Q. Ohtsuki. 1969. Control of muscle contraction. *Rev. Biophys.* 2:351–384.
2. Weber, A., R. Herz, and J. Reiss. 1963. On the mechanism of the relaxing effect of fragmented sarcoplasmic reticulum. *J. Gen. Physiol.* 46:679–702.
3. Duggan, P. F., and A. Martonosi. 1970. Sarcoplasmic reticulum. IX. Permeability of sarcoplasmic reticulum membranes. *J. Gen. Physiol.* 56:147–167.
4. Meissner, G., G. E. Conner, and J. Fleischer. 1973. Isolation of sarcoplasmic reticulum by zonal centrifugation and purification of Ca^{2+} pump and Ca^{2+} binding proteins. *Biochim. Biophys. Acta.* 298:246–269.
5. Herbette, L. G., J. Marquardt, A. Scarpa, and J. K. Blasie. 1977. A direct analysis of lamellar x-ray diffraction from hydrated oriented multilayers of fully functional sarcoplasmic reticulum. *Biophys. J.* 20:245–272.
6. Martonosi, A., and R. Feretos. 1964. Sarcoplasmic reticulum. I. The uptake of Ca^{2+} by sarcoplasmic reticulum fragments. *J. Biol. Chem.* 239:648–658.
7. Inesi, G. 1972. Active transport of calcium ions in sarcoplasmic membranes. *Annu. Rev. Biophys. Bioeng.* 1:191–210.
8. Palade, P., R. D. Mitchell, and S. Fleischer. 1983. Spontaneous calcium release from sarcoplasmic reticulum. *J. Biol. Chem.* 258:8089–8107.
9. Herbette, L. G., A. Scarpa, J. K. Blasie, C. T. Wang, A. Saito, and S. Fleischer. 1981. A comparison of the profile structures of isolated and reconstituted sarcoplasmic reticulum membranes. *Biophys. J.* 36:47–72.
10. Blasie, J. K., L. G. Herbette, P. H. DeFoor, and S. Fleischer. 1981. The profile structure of the Ca^{2+} pump protein molecule in the

isolated sarcoplasmic reticulum membrane. *Biophys. J.* 33(2, Pt. 2):228*a*. (Abstr.)

11. Herbette, L. G., and J. K. Blasie. 1980. Static and time-resolved structural studies on isolated sarcoplasmic reticulum membranes. *In* Calcium-Binding Proteins: Structure and Function. F. L. Siegel, E. Carafoli, R. H. Kretsinger, D. H. MacLennan, and R. H. Wasserman, editors. Elsevier North-Holland, Inc., New York. 115–120.
12. Blasie, J. K., L. G. Herbette, D. Pierce, D. Pascolini, A. Scarpa, and S. Fleischer. 1982. Static and time-resolved structural studies of the Ca^{2+}-ATPase of isolated sarcoplasmic reticulum. *Ann. NY Acad. Sci.* 402:478–484.
13. Blasie, J. K., L. G. Herbette, D. Pierce, D. Pascolini, V. Skita, A. Scarpa, and S. Fleischer. 1985. Static and time-resolved structural studies of the Ca^{2+}-ATPase of isolated sarcoplasmic reticulum. *In* Sarcoplasmic Reticulum: Structure and Function. S. Fleischer and Y. Tonomura, editors. Academic Press, Inc., New York. In press.
14. Herbette, L. G., P. DeFoor, S. Fleischer, D. Pascolini, A. Scarpa, and J. K. Blasie. 1985. The separate profile structures of the calcium pump protein and the phospholipid bilayer within isolated sarcoplasmic reticulum membranes determined by x-ray and neutron diffraction. *Biochim. Biophys. Acta.* In press.
15. McCray, J. A., L. G. Herbette, T. Kihara, and D. R. Trentham. 1980. A new approach to time-resolved studies of ATP-requiring biological systems: laser flash photolysis of caged ATP. *Proc. Natl. Acad. Sci. USA.* 77:7237–7241.
16. Pierce, D., A. Scarpa, M. R. Topp, and J. K. Blasie. 1983. Kinetics of calcium uptake by the sarcoplasmic reticulum vesicles using flash photolysis of caged adenosine 5'-triphosphate. *Biochemistry.* 22:5254–5261.
17. Pierce, D., A. Scarpa, D. R. Trentham, M. R. Topp, and J. K. Blasie. 1983. Comparison of the kinetics of calcium transport in vesicular dispersions and oriented multilayers of sarcoplasmic reticulum membranes. *Biophys. J.* 44:365–373.
18. Pierce, D. H. 1982. Ph.d. Dissertation, University of Pennsylvania. 126 pp.
19. MacLennan, D. H., and P. C. Holland. 1975. Calcium transport in sarcoplasmic reticulum. *Annu. Rev. Biophys. Bioeng.* 4:377–404.
20. de Meis, L., and A. L. Vianna. 1979. Energy interconversion by the Ca^{2+}-dependent ATPase of the sarcoplasmic reticulum. *Annu. Rev. Biochem.* 48:275–292.
21. Milch, J. R. 1979. Slow scan SIT detector for x-ray diffraction studies using synchrotron radiation. *IEEE (Inst. Electr. Electron. Eng.) Trans. Nucl. Sci.* NS-26:338–345.
22. Pachence, J. M., P. L. Dutton, and J. K. Blasie. 1981. The reaction center profile structure derived from neutron diffraction. *Biochim. Biophys. Acta.* 635:267–282.
23. Schwartz, S., J. E. Cain, E. Dratz, and J. K. Blasie. 1975. An analysis of lamellar diffraction from disordered membrane multilayers with application to data from retinal rods. *Biophys. J.* 15:1201–1233.
24. Pachence, J. M., P. L. Dutton, and J. K. Blasie. 1979. Structural studies of reconstituted reaction center/lecithin membranes. *Biochim. Biophys. Acta.* 548:348–373.
25. Winick, H., and S. Doniach. 1980. Synchrotron Radiation Research. Plenum Publishing Corp., New York. 754 pp.
26. Frankel, R. D., and J. M. Forsyth. 1983. The resolved x-ray diffraction studies of purple membrane from halobacterium halobium. *Biophys. J.* 41 (2, Pt. 2):15*a*. (Abstr.)
27. Fernandez-Belda, F., M. Kurzmack, and G. Inesi. 1984. A comparative study of calcium transients by isotopic tracer, metallochromic indicator and intrinsic fluorescence in sarcoplasmic reticulum ATPase. *J. Biol. Chem.* 259:9687–9698.